




A comparison of ZnO nanowires grown using hexamethylenetetramine and ammonium hydroxide on Al:ZnO nanoparticle seed layer

Ewan D. Matheson^{1,*} , Yongtao Qu¹, Giray Kartopu¹, Marc K. Etherington¹, Guillaume Zoppi¹, Vincent Barrioz¹, and Neil S. Beattie¹

¹Department of Mathematics, Physics and Electrical Engineering, Ellison Building, Northumbria University, Newcastle upon Tyne NE1 8ST, UK

Received: 1 June 2023

Accepted: 14 July 2023

Published online:
26 July 2023

© The Author(s) 2023

ABSTRACT

ZnO is a low-cost material which can be easily manipulated into different morphologies using hydrothermal synthesis. In this study, ZnO nanowires are grown using hexamethylenetetramine (HMTA) and ammonium hydroxide as bases for the hydrothermal method. The growth time and temperature are varied and the nanowires are characterised structurally and optically. Electron microscopy images of the nanowires show that ammonium hydroxide forms pointed tips whereas HMTA forms flat tips. This is attributed to the chelating properties of HMTA. X-ray diffraction patterns show strong *c*-axis preferred orientation exhibited by ammonium hydroxide grown nanowires with large variability in crystallinity, whereas HMTA produced nanowires that show random orientation. The optical band gap is observed to decrease with solution temperature for both types of bases, however surface oxygen vacancy defects are observed in photoluminescence measurements of the ammonium hydroxide grown nanowires.

1 Introduction

ZnO in the Wurtzite phase possesses a large direct band gap (3.37 eV), exciton energy (60 meV) and is suitable for gas sensors and many optoelectronic devices operating in the blue/UV region [1–4]. ZnO contains highly reactive ions meaning solution synthesis is possible as precipitate can easily form, resulting in many different morphologies such as

nanowires, nanoparticles, flower-like and cabbage-like nanostructures [5].

The hydrothermal method, shown in Fig. 1a, is a technique where precipitate forms on the seeded facet of a substrate [6]. The seed promotes the growth direction by matching the material density and structure. During this process, zinc nitrate ($\text{Zn}(\text{NO}_3)_2$) and ammonium hydroxide ($[\text{NH}_3^+][\text{OH}^-]$) precursors are often reacted in water and initially form a

Address correspondence to E-mail: ewan.matheson@northumbria.ac.uk

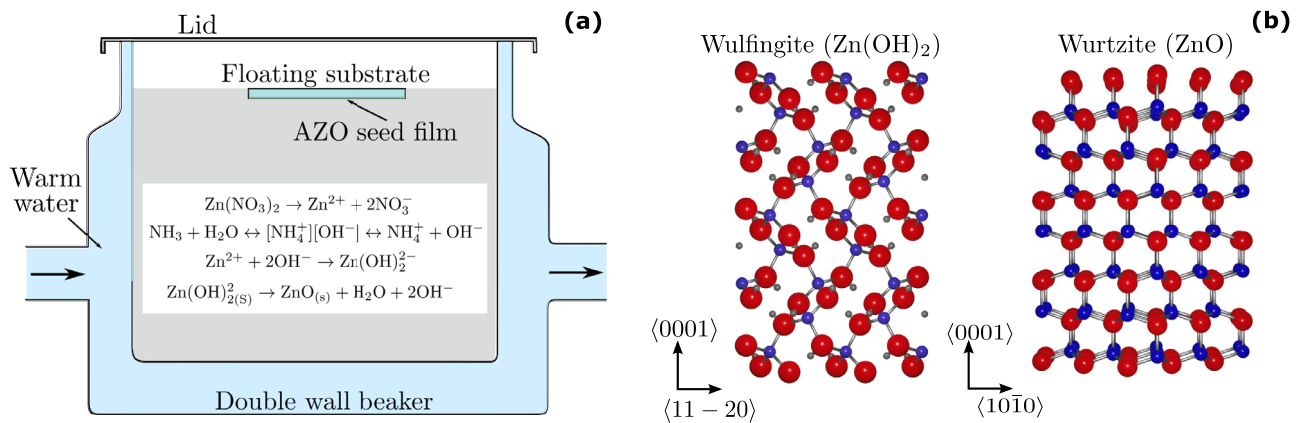


Fig. 1 **a** Hydrothermal method using a double walled beaker to control the solution temperature and **b** Wulffite and Wurtzite structures where blue atoms represent Zn, red represents O and grey represents H

precipitation of Wulffite $\text{Zn}(\text{OH})_2$ when the solution temperature is below 70°C , which after a period of time directly forms ZnO when the temperature increases [5, 7], shown in Fig. 1b. A similar effect can also be achieved using hexamethylenetetramine (HMTA, CH_2N_4), which hydrolyses and releases $[\text{NH}_3^+][\text{OH}^-]$ and formaldehyde (CH_2O). $[\text{NH}_3^+][\text{OH}^-]$ then provides the hydroxide ions (OH^-) for the formation of ZnO [8]. There are two pathways for $\text{Zn}(\text{OH})_2$ to form ZnO: dissolution and precipitation as ZnO, or solid state formation of ZnO. Of these two pathways, most of the oxygen does not mix with the water and thus ZnO forms mostly from crystallised $\text{Zn}(\text{OH})_2$.

The formation of $\text{Zn}(\text{OH})_2$ and ZnO varies with temperature such that as the temperature increases, the presence of ZnO also increases. It is hypothesised that low temperature solutions will be less suitable for nanowire growth [7]. Similarly, homogenous growth is achieved between a pH of 10 and 11 where equal concentration of OH^- to Zn^{2+} are present in the solution to allow precipitate to form [5]. It is also hypothesised that the rate by which OH^- is released into the solution will be different between $[\text{NH}_3^+][\text{OH}^-]$ and $(\text{CH}_2)_6\text{N}_4$ since the hydroxide ions are released directly from the ammonium hydroxide whereas the HMTA must first undergo a hydrolysis step.

In this study, we compared the formation of ZnO nanowires using ammonium hydroxide and HMTA bases and assessed their physical and optical properties as function of growth temperature and time. Previous research has shown ammonium hydroxide and HMTA are effective in the hydrothermal growth

of ZnO nanowires [9, 10], while this research discusses the differences between nanowires grown using these two bases. We chose a novel seed layer of aluminium doped zinc oxide (AZO) nanoparticle deposited by the slot-die method, illustrated in Fig. 2, for its promise for potential device applications in sensing and opto-electronics, as well as the significant difference in optical band gap exhibited by the nanoparticles to ensure true measurement of the nanowires.

2 Methods

2.1 Substrate and seed crystal

On a pre-cleaned $25\text{ mm} \times 75\text{ mm} \times 1\text{ mm}$ glass substrate, a thin film Al:ZnO (AZO) nanoparticle ($\sim 15\text{ nm}$ size) seed crystal was formed from a commercial (Avantama) ink using an Ossila slot-die coater, as described in Fig. 2. The ink is composed of

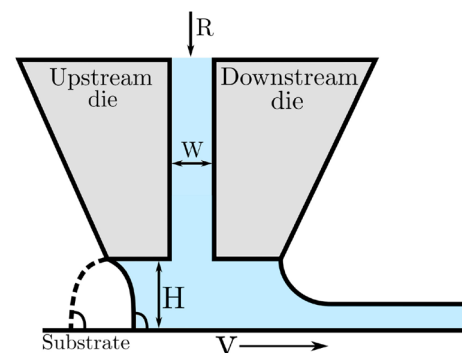


Fig. 2 Slot-die setup with flow rate R , slot width W , gap height H , coating speed V

a mixture of butanols. AZO was chosen as the seed film for ZnO nanowire growth as the optical band gap ($E_g = 4.37$ eV) is significantly different to the ZnO band gap ($E_g = 3.3$ eV), while having a similar crystal structure. This will minimise error associated with optical measurements of the nanowires. The slot-die coater was configured with coating speed, $V = 20$ mm/s, and ink flow rate at $R = 5.67$ $\mu\text{L/s}$. The slot width is determined by the thickness of the shim used, in this case being $W=100$ μm . The gap height, H , is positioned at 219 μm above the substrate surface to produce a 100 nm thick coating. These films were dried in air and used as deposited for consistency.

2.2 Hydrothermal growth

2.2.1 ZnO nanowires: ammonium hydroxide base

93.75 mL of 40 mM zinc nitrate solution is mixed with 56.25 mL of de-ionised water to make 150 mL of 25 mM zinc nitrate solution in a double-walled beaker. Ammonium hydroxide (NH_4OH) is rapidly added to adjust the pH to 9 and then drop-wise to reach a pH of 10. The substrate is floated on the solution surface, such that the seeded facet of the substrate is faced downwards. Four samples were synthesised at 50 °C, 60 °C, 70 °C and 80 °C solution temperatures for 90 min. A further three samples synthesised for 30, 45 and 60 min at 80 °C.

2.2.2 ZnO nanowires: HMTA base

The same 25 mM zinc nitrate solution is prepared in a double walled-beaker with a floating AZO seeded substrate. 0.525 g of HMTA is added to the solution to reach a pH of 10. Four samples were synthesised at 60 °C, 70 °C, 80 °C and 90 °C solution temperatures for 4 h. To study the nucleation-time dependence, further three samples were synthesised for 1 h, 2 h and 3 h at 90 °C. Higher temperature and longer growth time is used here to encourage the decomposition and hydrolysis of HMTA.

2.3 Characterisation measurements

The structural and optical measurements include scanning electron microscopy (SEM) using a Tescan Mira3 microscope to image the sample morphology and grazing incidence X-ray diffraction (GIXRD)

using a Rigaku SmartLab SE diffractometer (Cu K- α source) in parallel beam (PB) mode to identify crystal phase and size. A Shimadzu UV-2600 double beam spectrophotometer with a bare glass reference was used for UV-Vis absorption measurements to deduce the optical band gap. A HORIBA Fluorolog-QM with a 370 nm excitation source was used for room-temperature photoluminescence spectroscopy (PL) measurements.

3 Results and discussion

3.1 Ammonium hydroxide grown ZnO nanowires

Immediately upon adding the NH_4OH to the $\text{Zn}(\text{NO}_3)_2$ solution, a white precipitate begins to form, suggesting that the hydroxide ions dissipate into the solution quickly (~ 1 s). The pH rapidly increases from 7 to around 9 less than a second after adding ammonium hydroxide, confirming the release of hydroxide ions.

SEM images in Fig. 3a to h show the morphology of the nanowires grown at different temperatures using this technique. Plane view images show the nanowires are densely packed on the substrate surface with high uniformity. The diameter increases from around 50 nm to above 100 nm with growth temperature however the diameter varies significantly with both temperature and growth time and is attributed to the nucleation of the nanowires. At 80 °C they are well formed with smooth facets and sharp edges. The tips of the nanowires taper to a point, which suggests that as the ZnO precipitate increases, the concentration of $\text{Zn}(\text{NO}_3)_2$ and NH_4OH is reducing [11], restricting the non-polar growth of the nanowires. Time dependent experiments can reveal if the morphology of the tips form during or after the growth of the nanowires.

SEM images in Fig. 3i to n show the time dependency on the nanowires morphology. This reveals that the nanowires grow mostly in the early stage of the process and the tips are tapered throughout the growth. This suggests there are other mechanisms controlling the morphology. Figure 3o shows the tip aspect ratio, defined by the ratio of the width at the base of the tip to the height of the pyramid shape, exhibited throughout the growth process. Because the tip aspect ratio is non-zero after 30 min, the

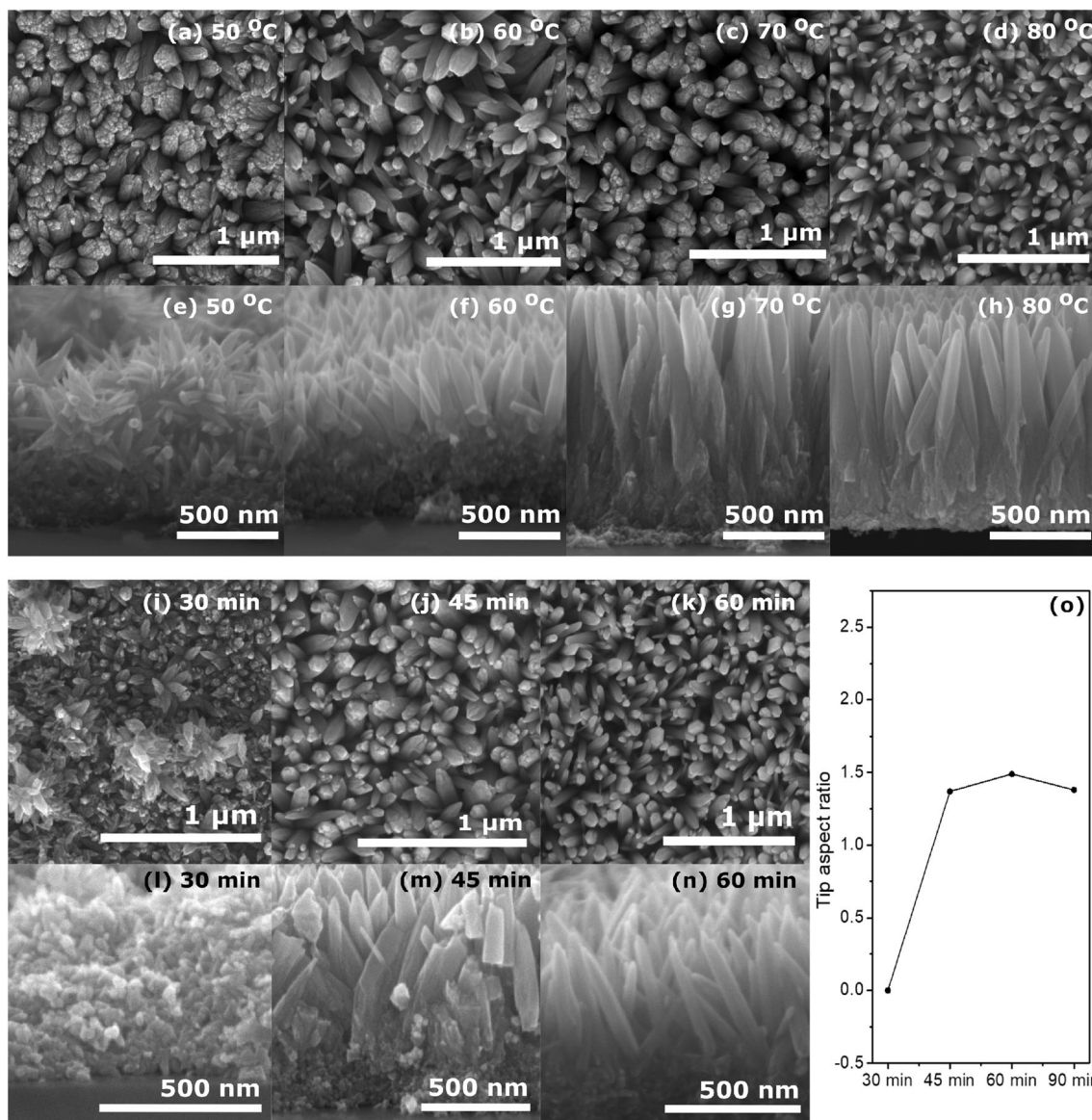


Fig. 3 SEM images of nanowires grown with **a** 50 °C, **b** 60 °C, **c** 70 °C and **d** 80 °C solution temperatures for 90 min at pH 10 with the corresponding cross sections in **e** to **h**. Nanowires grown

at 80 °C for **i** 30 min, **j** 45 min and **k** 60 min with the cross sections in **l** to **n**. The tip aspect ratio is shown in **o**

imbalance of the growth velocities of the hexagonal facets can be defined as $V_{(0001)} > V_{(1011)} > V_{(1010)}$ which leads to the pointed shape at the end of the c -axis [12]. Cross section SEM images show that the nanowires are well aligned at temperatures above 70 °C and increase in length with growth time and temperature, measuring below 500 nm below 70 °C and less than 45 min of growth, then reach a maximum length which varies between 600 nm and 1000 nm above 70 °C and longer than 45 min of growth.

The crystal structure and phase of the nanowires are illustrated in the XRD reflection patterns in Fig. 4.

For all samples measured, the peak positions match closely with ZnO Wurtzite structure. The synthesis solution temperature shown in Fig. 4a has a significant effect on the c -axis, indicated by the increasing intensity of the (002) peak with solution temperature. Crystallite size, shown in the Figure insets, is calculated using the Scherrer equation [13]:

$$\tau = \frac{K\lambda}{\beta \cos(\theta)} \quad (1)$$

where τ is the crystallite size, $\lambda = 0.15406$ nm (Cu K- α X-ray source), β is the average width at half

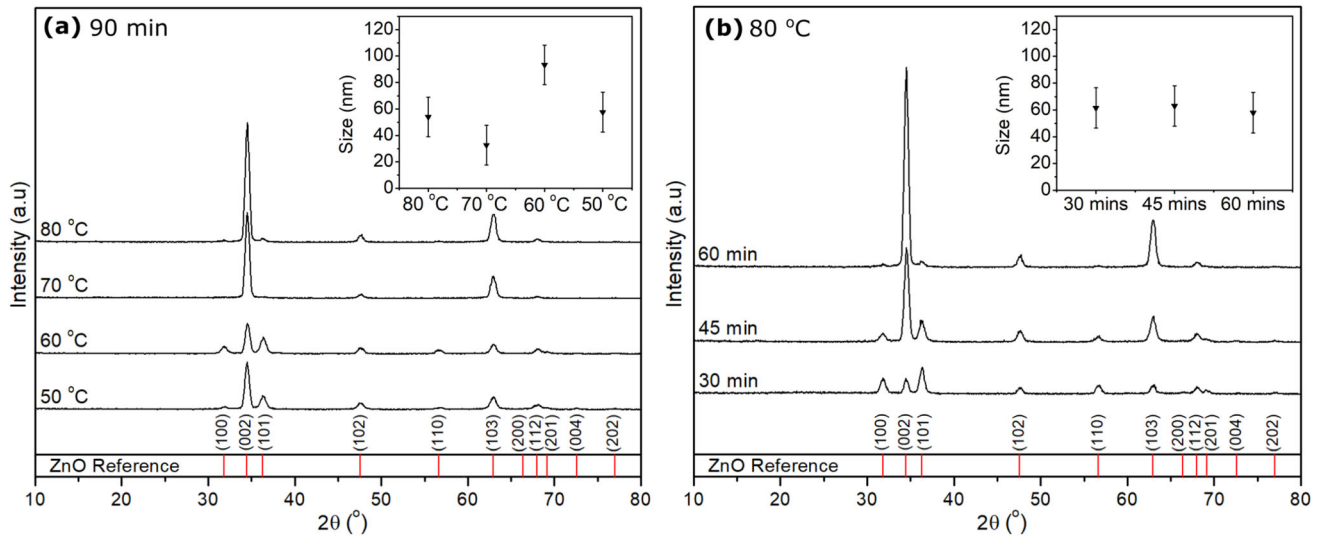


Fig. 4 XRD reflection patterns of nanostructures grown at different solution temperatures (a) and growth times (b). Wurtzite ZnO peak positions (ICSD: 193696) are shown as reference. The crystallite size calculated using the Scherrer equation is shown in the insets

maximum of the (100), (002), (102) and (103) peaks, θ is the Bragg angle of each peak and K is a constant. In other works, K has been found to vary between 0.62 and 2.08, however 0.8 to 1 is typically used when the crystal shape is unknown [14]. Using $K = 0.9 \pm 0.1$ gives an uncertainty of ± 15 nm on the crystallite size values. Additionally, the Williamson–Hall equation was used to calculate the relative strain however this was found to be no higher than 0.4% of the crystallite size and therefore has no significant contribution towards peak broadening [15].

Crystallite size shows no temperature dependence and varies significantly between 32.6 nm and 93.3 nm, however, in Fig. 4b, there is less variance with growth time at a given temperature (80 °C) which is measured between 61.5 and 54.4 nm. This is likely due to the similar growth conditions from the time-dependent samples. The c-axis peak intensity increases with growth time which is expected as the nanowires grow longer along the c-axis.

The texture coefficient (TC) was calculated to determine preferred orientation;

$$TC = \frac{n \left(\frac{I_i}{I_{oi}} \right)}{\sum_{i=1}^n \left(\frac{I_i}{I_{oi}} \right)} \quad (2)$$

where I_i is the peak intensity of the ZnO reference, I_{oi} is the measured peak intensity and n is the number of peaks used in the calculation. Table 1 demonstrates that the c-axis (002) is the preferred orientation of the

ZnO crystals and is maximised at temperatures above 70 °C and for longer than 60 min growth times.

UV–Vis absorption spectra were used to deduce the optical band gap of the nanowires grown at different temperatures and growth times as shown in Figs. 5a and b. From the Bouguer–Beer–Lambert law, the absorption coefficient α , is calculated using [16]:

$$\alpha = \frac{A_{abs}}{d} \quad (3)$$

where d is optical path length and A_{abs} is the quantity of absorbed light defined as;

$$A_{abs} = -\ln \left[\frac{T(\lambda)}{I(\lambda) - R(\lambda)} \right] \quad (4)$$

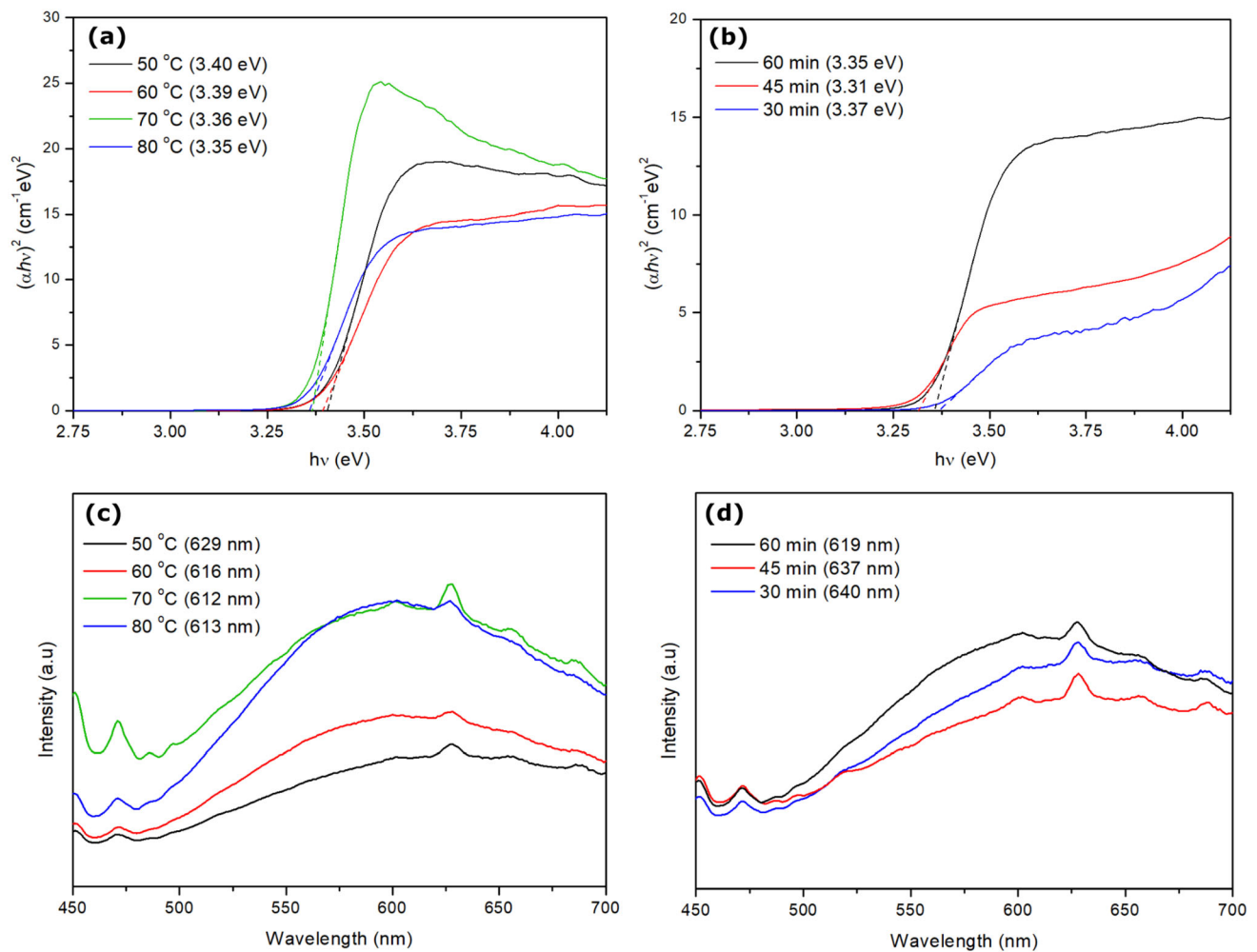
where λ is wavelength, $T(\lambda)$ is the intensity of transmitted light, $I(\lambda)$ is the intensity of the incident light and $R(\lambda)$ is the intensity of reflected light. Approximately 4% of incident light is reflected from the glass calculated using the Fresnel equation, therefore A_{abs} can be simplified to depend only on $T(\lambda)$. The optical band gap is then deduced using Eqs. 3 and 4, with the Tauc equation [17]:

$$(\alpha h\nu)^{\frac{1}{\gamma}} = B(h\nu - E_g) \quad (5)$$

where h is Planck’s constant, ν is the photon frequency, B is a constant related to band edge tailing and E_g is the optical band gap. For direct band gaps, $\gamma = \frac{1}{2}$ which is constant for this type of exciton transition. The measured optical band gaps vary around the bulk band gap for ZnO [18] at 3.37 eV, reducing

Table 1 Texture coefficients of ammonium hydroxide grown ZnO nanowires

Peak	50 °C	60 °C	70 °C	80 °C	30 min	45 min	60 min
(100)	0.12	0.41	0.00	0.04	0.98	0.20	0.06
(002)	2.57	2.14	2.91	2.90	1.54	2.52	2.91
(102)	0.58	0.69	0.25	0.29	0.29	0.51	0.43
(103)	0.72	0.76	0.84	0.76	0.71	0.77	1.15

**Fig. 5** UV–Vis absorption spectrum of ZnO nanowires grown at temperatures ranging from 50 to 80 °C shown in **(a)** and growth times ranging from 30 min to 1 h shown in **(b)** with band gap

energies. Corresponding room temperature PL emission spectra shown in **c** and **d** with visible peak positions

with temperature from 3.40 to 3.35 eV and varying with growth time between 3.31 and 3.37 eV. Variation in band gap transition energies are associated with excitons bound to neutral or charged donor or acceptors [19], suggesting that solution temperature and growth time may have an effect on the nature of these sites.

Figure 5c and d show the PL spectra for the corresponding ZnO nanowires grown using ammonium

hydroxide. ZnO typically has two PL emission bands: the band-to-band (BB) emission peak which lies in the UV-region (shown in appendix Fig. 9) and the deep level (DL) emission peak which lies in the visible region and is associated with electron–hole recombination caused by intrinsic point defects such as oxygen vacancies (V_{O}), zinc interstitials (Zn_i) and the incorporation of hydroxyl groups in the crystal lattice during the growth process [20]. Since

Table 2 Ratio of DL emission to band-to-band peak intensities for ammonium hydroxide grown nanowires

Sample	$I_{DL} \times 10^6$ (a.u)	$I_{BB} \times 10^7$ (a.u)	I_{DL}/I_{BB}
50 °C	3.3	1.7	0.19
60 °C	4.4	2	0.22
70 °C	7.3	3.6	0.21
80 °C	7.2	1.1	0.66
30 min	5.1	2.6	0.19
45 min	4.2	2.9	0.14
60 min	5.8	1.9	0.30

nanowires have a high surface to volume ratio, the visible peak likely originates from the surface region which suggests that the associated defects are likely surface states [21]. Previous research has shown that V_O are the dominant donor-like point defects responsible for the ZnO n-type conductivity [22], however it is also likely that the n-type conductivity may be from unintentional shallow donors such as hydrogen which is present in almost all processing conditions [23].

The peak intensity appears to increase with growth time and temperature. This may be due to either changes in material bulk density related to nanowire packing which results in different defect densities, or only a change in defect density with changing growth conditions. To verify this, the ratio of the DL peak intensity (I_{DL}) to the bulk band-to-band peak intensity (I_{BB}) can be calculated to account for changes in bulk density as shown in Table 2. This qualitatively shows that V_O or Zn_i defect emission increases with solution temperature and growth time relative to the band-to-band emission which may be attributed to water forming during the reaction process [24].

3.2 HMTA grown ZnO nanowires

Immediately after adding HMTA to the $Zn(NO_3)_2$ solution at room temperature, the HMTA dissolves rapidly however there is no colour change or precipitate forming in the solution. There is also no change in pH during this step. This shows that the thermal decomposition of HMTA into ammonium hydroxide and formaldehyde does not occur. When the hot bath is connected, the white precipitate begins to form as the temperature of the solution increases.

SEM images in Fig. 6a to h show the plane view and cross section morphology of the nanowires

grown at temperatures ranging from 60 to 90 °C. The nanowires are randomly orientated on the substrate compared to the ammonium hydroxide grown nanowires, which is possibly a result of longer exposure of the nanoparticle seed layer to the solution disturbing the morphology of the surface. The nanowire length increases with solution temperature from around 300 nm at 70 °C to over 500 nm at 90 °C. There is large variability in diameter of the HMTA grown nanowires, ranging from 20 nm to 100 nm. Below 70 °C the hydrolysis of HMTA to ammonium hydroxide is slow and ZnO does not form in the solution. Due to HMTA being a non-polar chelating agent, only the (002) growth direction is exposed for epitaxial growth, giving these nanowires a high aspect ratio near the tips [25] causing them to appear flat, compared to the pointed tips of the ammonium hydroxide grown nanowires.

SEM images in Fig. 6i to n show plane view and cross section of the nanowire growth over time and reveal flat tips throughout the growth process. The length increases over time from 150 nm after 1 h to 200 nm after 3 h, however there is variation between the cross section and plane view images, with plane view showing lengths of around 500 nm.

The crystal structure and phase of the HMTA grown nanowires are represented in the XRD reflection patterns in Fig. 7. The peak positions match closely with ZnO Wurtzite structure, which is truly reflected in the SEM images in Fig. 6 where the hexagonal shape of the nanowire tips can be observed. Crystallinity calculations shown in the insets of Fig. 7a and b, suggest that the crystallinity improves with solution temperature, however there is large variation in the measurements similar to the ammonium hydroxide samples and likely results from the variation in the uniformity of the precipitate in the solution. Figure 7b also shows increasing peak intensity and less variation in crystallinity with growth time, similar to that displayed by the ammonium hydroxide grown nanowires.

Texture coefficient calculations shown in Table 3, suggest these nanowires are randomly orientated, and that increasing the growth time above 3 h at 90 °C improves the (002) orientation.

Figure 8a and b show the UV–Vis absorption spectrum of the HMTA grown nanowires. The band gap is observed to decrease with growth temperature from 3.30 to 3.28 eV, slightly lower than expected for ZnO at 3.37 eV. This suggests that growth

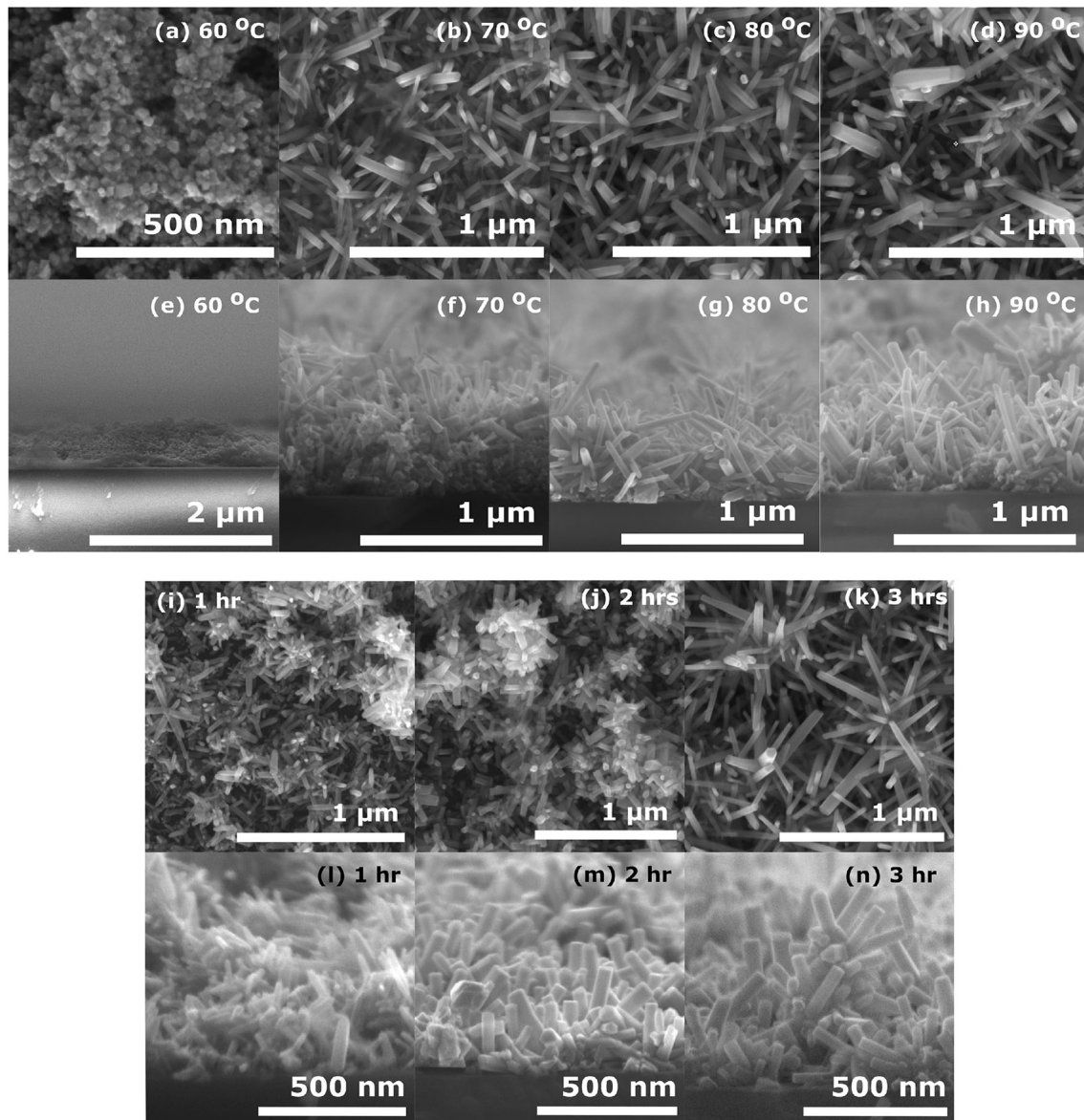


Fig. 6 SEM images of nanowires grown with **a** 60 °C, **b** 70 °C, **c** 80 °C and **d** 90 °C solution temperatures for 4 h with the corresponding cross sections in **e** to **h**. Nanowires grown for **i** 1 h, **j** 2 h and **k** 3 h are shown below with the cross sections shown in **l** to **n**

temperature affects the nature of the excitons bound to charged donor and acceptor sites, similar to that displayed by the ammonium hydroxide samples. The growth time varies the band gap, which is measured between 3.28 and 3.30 eV.

Figure 8c and d show the PL spectra of the ZnO nanowires. The ratio of the DL to band-to-band peaks can be calculated to examine if the change in intensity can be attributed to defect density, similar to the method employed for analysing Fig. 5. The ratios are listed in Table 4. The peak ratios are significantly

lower than those listed in Table 2, suggesting that HMTA produces ZnO nanowires with a lower concentration of V_O . The ammonium hydroxide curve shown in Figs. 8c and d qualitatively illustrates this showing a more intense peak relative to the HMTA grown samples. The solution temperature and growth time increases the V_O or Zn_i concentration in the HMTA grown samples similar to that observed with ammonium hydroxide, therefore this may also be from water formation during the reaction.

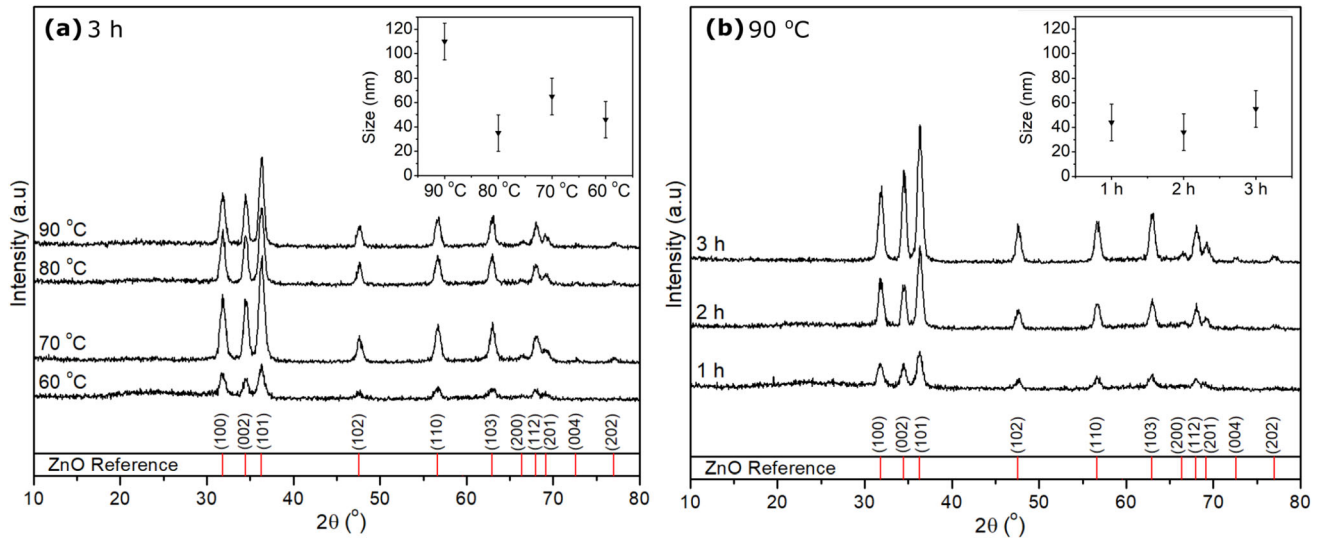


Fig. 7 XRD patterns of HMTA grown ZnO with **a** different solution temperature and **b** different growth times. ZnO peak positions (ICSD: 193696) are shown as a reference. The crystallite size calculated using the Scherrer equation is shown in the insets

Table 3 Texture coefficients of HMTA grown ZnO nanowires

Peak	60 °C	70 °C	80 °C	90 °C	1 h	2 h	3 h
(100)	1.08	1.02	1.02	0.99	1.40	1.52	1.29
(002)	1.16	1.23	1.17	1.25	1.81	1.73	2.02
(102)	0.99	0.88	0.96	0.89	1.51	1.39	1.48
(103)	0.76	0.87	0.85	0.87	1.27	1.36	1.21

4 Conclusion

Zinc oxide nanowires were fabricated on Al:ZnO nanoparticle seed films using ammonium hydroxide and HMTA as ion bases. Ammonium hydroxide releases ions rapidly into the solution, forming the ZnO precipitate faster than HMTA, confirming the hypothesis regarding this mechanism. This results in faster growth and significantly different morphologies, particularly at the nanowire tips. Further, long growth times using HMTA disturbs the nanoparticle film causing the nanowires to grow in different directions relative to the substrate surface.

Solution temperature affects the growth of the nanowires significantly. SEM images show an increase in nanowire formation with temperature for both growth processes. XRD analysis shows an increase of preferred orientation of ammonium hydroxide nanowires with solution temperature suggesting better nanowire alignment which is reflected in the SEM cross section images. Further, PL

shows qualitatively an increase in oxygen vacancy defects with solution temperature for both growth methods while spectrophotometry shows a slight reduction in band gap with temperature for ammonium hydroxide grown nanowires. This reflects the hypothesis that increased solution temperature is beneficial for nanowire growth.

Longer growth time is overall beneficial. The nanowires form in the early stages of the growth process for both methods, however show improved optical and structural characteristics in the later stages of growth.

Optical measurements indicate slight variation of optical band gap likely caused by excitons bound to charged and neutral donors or acceptors, with ammonium hydroxide producing a wider ZnO band gap than HMTA by around 0.05 eV. PL measurements show a large difference in deep level emission between the two methods, where defects such as oxygen vacancies near the surface, are formed using ammonium hydroxide.

Based on these results, the ammonium hydroxide synthesis of ZnO nanowires grown on novel AZO nanoparticle seed film results in high quality nanowires for optoelectronic applications. This includes high-quality optical properties, preferential orientation and relatively uniform growth. The use of a solution-processed AZO seed layer to achieve these properties provides a stable and low-cost alternative to physical vapour deposition techniques that demonstrates potential for incorporation into devices.

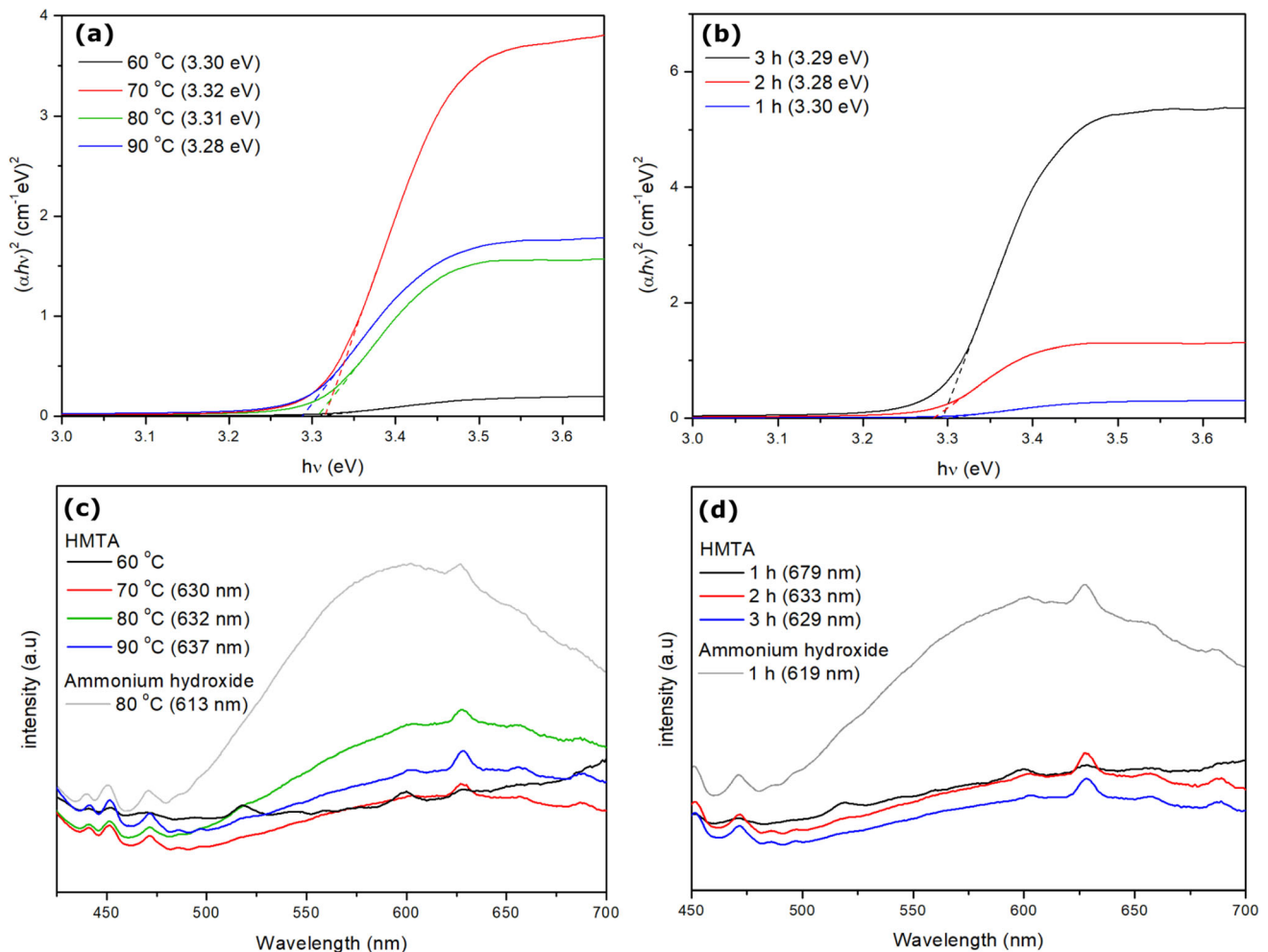


Fig. 8 UV–Vis absorption spectrum of HMTA grown ZnO nanowires with solution temperatures ranging from 60 to 90 °C shown in (a) and growth times ranging from 1 to 3 h shown in

b. Corresponding PL emission spectra shown in c and d featuring the emission of the 80 °C and 1 h ammonium hydroxide grown ZnO samples

Table 4 Ratio of DL emission to band-to-band peak intensities for HMTA grown nanowires

Sample	$I_{DL} (\times 10^6)$ (a.u)	$I_{BB} (\times 10^7)$ (a.u)	I_{DL}/I_{BB} (a.u)
60 °C	2.2	3.4	0.06
70 °C	2.0	2.4	0.08
80 °C	3.8	3.0	0.12
90 °C	2.7	3.5	0.08
1 h	2.0	3.7	0.06
2 h	4.2	2.9	0.08
3 h	5.8	2.0	0.09

Future research should address the stability of solution processed nanoparticle seed layer surfaces during HMTA nanowire growth.

Acknowledgements

We acknowledge support from the UK Engineering and Physical Sciences Research Council Grants EP/S023836/1, EP/T005491/1 and EP/W010062/1.

Author contributions

All authors contributed to the study conception and design. Material preparation, data collection and analysis were performed by Ewan Matheson. The first draft of the manuscript was written by Ewan Matheson and all authors commented on previous versions of the manuscript. All authors read and approved the final manuscript. **Data availability**

The datasets generated during and/or analyzed during the current study are available from the corresponding author on reasonable request.

Declarations

Conflict of interest The authors have no conflict of interest to declare.

Open Access This article is licensed under a Creative Commons Attribution 4.0 International License, which permits use, sharing, adaptation, distribution and reproduction in any medium or format, as long as you give appropriate credit to the original author(s) and the source, provide a link to the Creative Commons licence, and indicate if changes were made. The images or other third party material in this article are included in the article's

Creative Commons licence, unless indicated otherwise in a credit line to the material. If material is not included in the article's Creative Commons licence and your intended use is not permitted by statutory regulation or exceeds the permitted use, you will need to obtain permission directly from the copyright holder. To view a copy of this licence, visit <http://creativecommons.org/licenses/by/4.0/>.

Appendix

This section provides the full photoluminescence spectra (PL), shown in Fig. 9, for the calculation of the ratio of the deep level peak intensity (I_{DL}) to the band-to-band peak intensity (I_{BB}). The intensity of

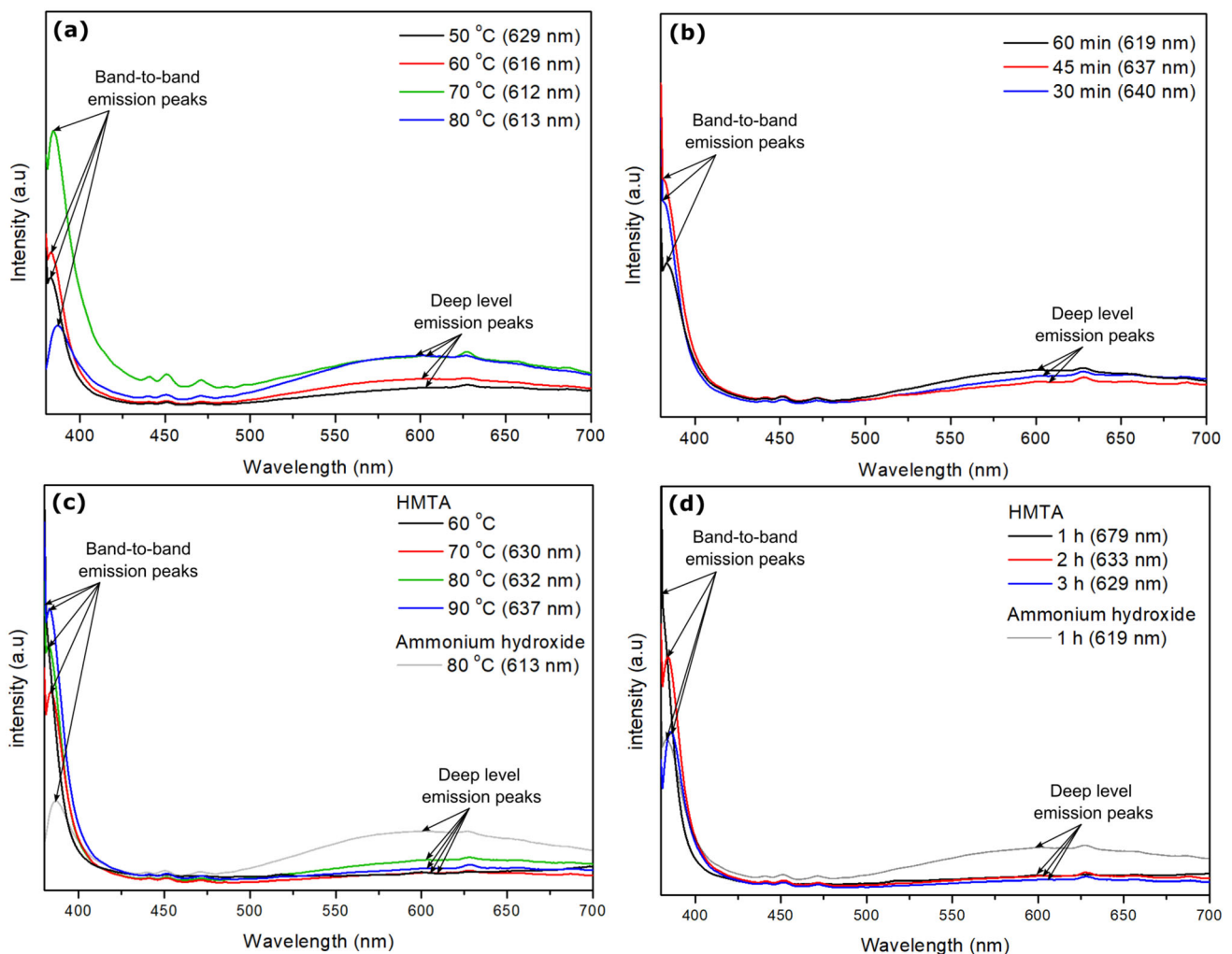


Fig. 9 Full PL spectra indicating the band-to-band peaks (BB) and the deep level emission peaks (DL)

both peaks for each sample is measured and the ratio is calculated as I_{DL}/I_{BB} .

References

1. S. Chu, G. Wang, W. Zhou, Y. Lin, L. Chernyak, J. Zhao, J. Liu, Electrically pumped waveguide lasing from ZnO nanowires. *Nat. Nanotechnol.* **6**(8), 506–510 (2011). <https://doi.org/10.1038/nnano.2011.97>
2. J.H. Na, M. Kitamura, M. Arita, Y. Arakawa, Hybrid p–n junction light-emitting diodes based on sputtered ZnO and organic semiconductors. *Appl. Phys. Lett.* **95**(25), 1–4 (2009). <https://doi.org/10.1063/1.3275802>
3. T.F. Choo, N.U. Saidin, K.Y. Kok, Hydrogen sensing enhancement of zinc oxide nanorods via voltage biasing. *R. Soc. Open Sci.* (2018). <https://doi.org/10.1098/rsos.172372>
4. G. Kartopu, D. Turkyay, C. Ozcan, W. Hadibrata, P. Aurang, S. Yerci, S.J.C. Irvine et al., Photovoltaic performance of CdS/CdTe junctions on ZnO nanorod arrays. *Solar Energy Mater. Solar Cells* **176**(December 2017), 100–108 (2018). <https://doi.org/10.1016/j.solmat.2017.11.036>
5. S. Baruah, J. Dutta, Hydrothermal growth of ZnO nanostructures. *Sci. Technol. Adv. Mater.* (2009). <https://doi.org/10.1088/1468-6996/10/013001>
6. N.T. Son, J.S. Noh, S. Park, Role of ZnO thin film in the vertically aligned growth of ZnO nanorods by chemical bath deposition. *Appl. Surf. Sci.* **379**, 440–445 (2016). <https://doi.org/10.1016/j.apsusc.2016.04.107>
7. N.J. Nicholas, G.V. Franks, W.A. Ducker, The mechanism for hydrothermal growth of zinc oxide. *CrystEngComm* **14**(4), 1232–1240 (2012). <https://doi.org/10.1039/c1ce06039b>
8. R. Parize, J. Garnier, O. Chaix-Pluchery, C. Verrier, E. Appert, V. Consonni, Effects of hexamethylenetetramine on the nucleation and radial growth of ZnO nanowires by chemical bath deposition. *J. Phys. Chem. C* **120**(9), 5242–5250 (2016). <https://doi.org/10.1021/acs.jpcc.6b00479>
9. S. Lee, J.K. Kim, S. Lee, J.K. Kim, Surface-enhanced Raman spectroscopy (SERS) based on ZnO nanorods for biological applications. *Zinc Oxide Based Nano Mater. Devices* (2019). <https://doi.org/10.5772/INTECHOPEN.84265>
10. T. Demes, C. TERNON, D. Riassetto et al., Comprehensive study of hydrothermally grown ZnO nanowires. *J. Mater. Sci.* **51**, 10652–10661 (2016). <https://doi.org/10.1007/s10853-016-0287-8>
11. S. Boubenia, A.S. Dahiya, G. Poulin-Vittrant, F. Morini, K. Nadaud, D. Alquier, A facile hydrothermal approach for the density tunable growth of ZnO nanowires and their electrical characterizations. *Sci. Rep.* **7**(1), 1–10 (2017). <https://doi.org/10.1038/s41598-017-15447-w>
12. Z. Zhang, J. Mu, Hydrothermal synthesis of ZnO nanobundles controlled by PEO–PPO–PEO block copolymers. *J. Colloid Interface Sci.* **307**(1), 79–82 (2007). <https://doi.org/10.1016/j.jcis.2006.10.035>
13. L. Alexander, H.P. Klug, Determination of crystallite size with the X-ray spectrometer. *J. Appl. Phys.* **21**(2), 137–142 (1950). <https://doi.org/10.1063/1.1699612>
14. V. Uvarov, I. Popov, Metrological characterization of X-ray diffraction methods at different acquisition geometries for determination of crystallite size in nano-scale materials. *Mater. Charact.* **85**, 111–123 (2013). <https://doi.org/10.1016/j.matchar.2013.09.002>
15. V. Mote, Y. Purushotham, B. Dole, Williamson–Hall analysis in estimation of lattice strain in nanometer-sized ZnO particles. *J. Theor. Appl. Phys.* **6**, 6 (2012). <https://doi.org/10.1186/2251-7235-6-6>
16. I. Mills, T. Cvitas, K. Homann, N. Kallay, K. Kuchitsu, IUPAC green book. (2007). <https://doi.org/10.1039/9781847557889>
17. P. Makuła, M. Pacia, W. Macyk, How to correctly determine the band gap energy of modified semiconductor photocatalysts based on UV–Vis spectra. *J. Phys. Chem. Lett.* **9**(23), 6814–6817 (2018). <https://doi.org/10.1021/acs.jpclett.8b02892>
18. K. Davis, R. Yarbrough, M. Froeschle, J. White, H. Rathnayake, Band gap engineered zinc oxide nanostructures: via a sol–gel synthesis of solvent driven shape-controlled crystal growth. *RSC Adv.* **9**(26), 14638–14648 (2019). <https://doi.org/10.1039/c9ra02091h>
19. A. Galdámez-Martínez, G. Santana, F. Güell, P.R. Martínez-Alanis, A. Dutt, Photoluminescence of ZnO nanowires: a review. *Nanomaterials* (2020). <https://doi.org/10.3390/nano10050857>
20. D. Raoufi, Synthesis and photoluminescence characterization of ZnO nanoparticles. *J. Lumin.* **134**, 213–219 (2013). <https://doi.org/10.1016/j.jlumin.2012.08.045>
21. S. Pramanik, S. Mondal, A.C. Mandal, S. Mukherjee, S. Das, T. Ghosh, P.K. Kuir, Role of oxygen vacancies on the green photoluminescence of microwave-assisted grown ZnO nanorods. *J. Alloys Compd.* **849**, 156684 (2020). <https://doi.org/10.1016/j.jallcom.2020.156684>
22. L. Liu, Z. Mei, A. Tang, A. Azarov, A. Kuznetsov, Q.K. Xue, X. Du, Oxygen vacancies: the origin of n-type conductivity in ZnO. *Phys. Rev. B* **93**(23), 1–7 (2016). <https://doi.org/10.1103/PhysRevB.93.235305>
23. A. Janotti, C.G. van de Walle, Fundamentals of zinc oxide as a semiconductor. *Rep. Prog. Phys.* **72**, 29 (2009). <https://doi.org/10.1088/0034-4885/72/12/126501>

24. V. Gurylev, T.P. Perng, Defect engineering of ZnO: review on oxygen and zinc vacancies. *J. Eur. Ceram. Soc.* **41**(10), 4977–4996 (2021). <https://doi.org/10.1016/J.JEURCERAMSOC.2021.03.031>
25. A. Sugunan, H.C. Warad, M. Boman, J. Dutta, Zinc oxide nanowires in chemical bath on seeded substrates: role of hexamine. *J. Sol–Gel Sci. Technol.* **39**(1 SPEC. ISS), 49–56 (2006). <https://doi.org/10.1007/s10971-006-6969-y>

Publisher's Note Springer Nature remains neutral with regard to jurisdictional claims in published maps and institutional affiliations.